Article

Photodynamic Therapy with an AlPcS₄Cl Gold Nanoparticle Conjugate Decreases Lung Cancer's Metastatic Potential

Anine Crous *[iD] and Heidi Abrahamse *[iD]

Laser Research Centre, Faculty of Health Sciences, University of Johannesburg, P.O. Box 17011,
Johannesburg 2028, South Africa
* Correspondence: acrous@uj.ac.za (A.C.); habrahamse@uj.ac.za (H.A.)

Abstract: Cancer metastasis and the risk of secondary tumours are the leading causes of cancer related death, and despite advances in cancer treatment, lung cancer remains one of the leading causes of death worldwide. A crucial characteristic of metastases is cell invasion potential, which is mainly determined by cell motility. Photodynamic therapy (PDT), known for its minimally invasive cancer treatment approach, has been extensively researched in vitro and is currently being developed clinically. Due to their physicochemical and optical properties, gold nanoparticles have been shown to increase the effectivity of PDT by increasing the loading potential of the photosensitizer (PS) inside cancer cells, to be biocompatible and nontoxic, to provide enhanced permeability and retention, and to induce lung cancer cell death. However, effects of gold nano phototherapy on lung cancer metastasis are yet to be investigated. The aim of this in vitro study was to determine the inhibitory effects of PS-gold nano bioconjugates on lung cancer metastasis by analysing cell proliferation, migration, cell cycle analysis, and extracellular matrix cell invasion. The findings indicate that nano-mediated PDT treatment of lung cancer prevents lung cancer migration and invasion, induces cell cycle arrest, and reduces lung cancer proliferation abilities, elaborating on the efficacy of the nano-mediated PDT treatment of lung cancer.

Keywords: phototherapy; photodynamic therapy; gold nanoparticles; drug delivery; lung cancer; metastasis

1. Introduction

Cancer metastasis refers to the spread of cancer cells to organs and tissues other than the tumour's original site of origin, as well as to the formation of new tumours [1]. When tumour cells acquire the potential to infiltrate neighbouring tissues, the invasion process begins with their migration through the extracellular matrix (ECM), eventually resulting in intravasation once they reach the circulatory system. Extravasation occurs when metastatic cells invade the vascular ECM as they transit through the circulatory system. These cells can eventually attach to a new location and proliferate to form the secondary tumour. The sequence of processes resulting in malignancy has a vital role in determining the prognosis of cancer patients. The process known as tumour metastasis occurs when a primary tumour spreads to other organs, and it is the leading cause of cancer death and morbidity [1]. With an estimated 1.8 million deaths, cancers of the lung continue to be the most common cause of cancer-related deaths worldwide [2]. Despite significant diagnostic and therapeutic advances, the impact on mortality has been modest, and, overall, survival remains low. Lung cancer is very heterogeneous, with many subtypes that have pathological and clinical significance. One of the reasons for its high mortality rate is that about 70% of lung cancer patients are diagnosed with advanced-stage disease [3]. Lung cancer treatment choices differ depending on the form and stage of the cancer, as well as its size and location in the lung. Treatment is also determined by whether the cancer has spread to other areas of the body and the patient's overall physical health. However,

most traditional lung cancer treatment options have negative side effects. This is where research can concentrate on developing a drug that can efficiently destroy cancer, reduce cancer progression and metastasis, and have little or no side effects. Photobiomodulation (PBM) is a form of phototherapy that uses low powered irradiation to induce a molecular reaction in cells depending on the wavelength used [4]. Red light can effectively penetrate tissue and is absorbed by cellular chromophores. This light stimulation can lead to ATP production and physiological increases in reactive oxygen species that can promote cell proliferation and migration [5]. When combining PBM with a photosensitizer, the therapy becomes what is known as photodynamic therapy (PDT). PDT, a form of phototherapy using photoactivated sensitising chemicals in conjunction with molecular oxygen, also known as alternate/photo chemotherapy, is a non-invasive, advanced method of cancer treatment that is usually performed as an outpatient procedure that can be used sequentially or in combination with conventional cancer treatments [6]. In the PDT mechanism of action, the photosensitive chemical is stimulated by photon absorption from a particular light wave. The excited photosensitizer (PS) generates oxidants, which damage cell membranes and kill cells [7]. Aluminium (III) Phthalocyanine Chloride Tetra sulphonate (AlPcS$_4$Cl) is a second-generation PS that exhibits superior PDT characteristics. Phthalocyanines (Pc) are red-absorbing dyes, having a high molar absorption coefficient. Pcs are second-generation PSs with a high extinction coefficient between 670 and 750 nm and up to 1000 nm. As a result, the initiating light penetrates further into the tissue [8]. Furthermore, it has an increased triplet state lifetime (τ t), yield (Φt), and singlet oxygen yield ($\Phi\Delta$) [9], is soluble in polar solvents such as water and has the ability to attach to mitochondrial cytochrome c, making it amphiphilic; it also exhibits no toxicity in the absence of photoactivation [8]. Despite advances in the usage of PDT for cancer treatment, problems such as nonspecific PS absorption and drug distribution remain unresolved [10]. Rapidly developing science is employing nanoparticles (NPs) to overcome cancer drug toxicity and a lack of specificity, enhance drug capacity as well as bioavailability where studies have shown improved concentration of the therapeutic agent in cancer cells as well as regulated drug release when NPs are used as drug delivery vehicles [11,12]. The use of NPs is encouraged, attributed to their distinctive physical, chemical, and biological characteristics such as polydispersity, stabilization, and biocompatibility [13]. Metallic NPs are from a variety of different metals, the nanoscale size causes electron confinement, which results in surface plasmon resonance. Gold and silver are the most-used NPs due to their unique physical properties of being less reactive and more stable in air, offering a large surface area and high level of conductivity, chemical stability, catalytic activity, and their antimicrobial activity [14]. Although silver nanoparticles produce stronger plasmon resonance than gold [15], making them popular for use in medical and electrical applications, gold nanoparticles (AuNPs) are more popular, as silver nanoparticles tend to oxidise easier than gold [16], making them too unstable for biomedical applications. AuNPs exhibit precise physicochemical and optical properties; as the least active metal, gold has extremely stable chemical properties, is nontoxic, and has a high biocompatibility; they also exhibit enhanced permeability and retention [17]. AuNPs are also used in advanced applications because of their ability to be synthesized at the nanoscale and functionalized with thiol and amine groups, allowing for the conjugation of various functional groups such as targeted antibodies or drug products [18].

It has been proven that AuNP-mediated PDT can effectively induce cell death in lung cancer [19]. However, nano-mediated PDT effects on lung cancer metastasis are yet to be investigated. The objective of this in vitro research was to ascertain the inhibitory effects of a PS-gold nano bioconjugate on lung cancer metastasis by analysing cell proliferation, migration, cell cycle analysis, and ECM invasion.

2. Materials and Methods

2.1. Cell Culture

Commercially available cancer cells received from the ATCC® (Manassas, VA, USA) were used in this study. Lung cancer cells, A549 (ATCC® CCL-185™, Manassas, VA, USA),

were cultured in complete media consisting of Roswell Park Memorial Institute 1640 base medium (RPMI-1640) with 10% heat inactivated Gibco foetal bovine sera (Gibco; 10082147) and antibiotic (penicillin/streptomycin [10 mL/L] (Sigma; P0781, St. Louis, MO, USA) and amphotericin B [2.5 mg/L] (Sigma; A2411, St. Louis, MO, USA)) additives. All cultured cells were maintained and incubated at 37 °C in 5% CO_2 and 85% humidity (Heracell™ 150i CO_2 Incubator, Thermo Scientific™, 51026280, Waltham, MA, USA), where they were cultured in Corning® cell culture flasks (Sigma, CLS430639/CLS430641/CLS431080, St. Louis, MO, USA).

2.2. Photodynamic Treatment

The AlPcS$_4$Cl-goldnano bioconjugate that was used in this study has been previously synthesized and characterised as described, where the PS, AlPcS$_4$Cl (Frontier Scientific, AlPcS-834, Logan, UT, USA), was adsorbed onto AuNP-PEG-COOH (Sigma–Aldrich, 765465, St. Louis, MO, USA). The physicochemical properties of the AlPcS$_4$Cl-AuNP-PEG-COOH conjugate include a mean diameter of 61.99 nm, a polydispersity index of 0.477, and zeta potential of -2.7 [19]. For this experiment, cells were grown in a 3.5 cm petri dish at a density of 5×10^5 cells and permitted to adhere for four hours prior to being exposed to PS and PS conjugate at a concentration of 20 µM; AlPcS4Cl was established as the [IC50] [20]. Experiments were divided into 4 groups, including an untreated control group, cells receiving PBM alone, cells receiving PDT using AlPcS$_4$Cl, and cells treated with nanoPDT using the AlPcS$_4$Cl gold nanoparticle conjugate (Figure 1).
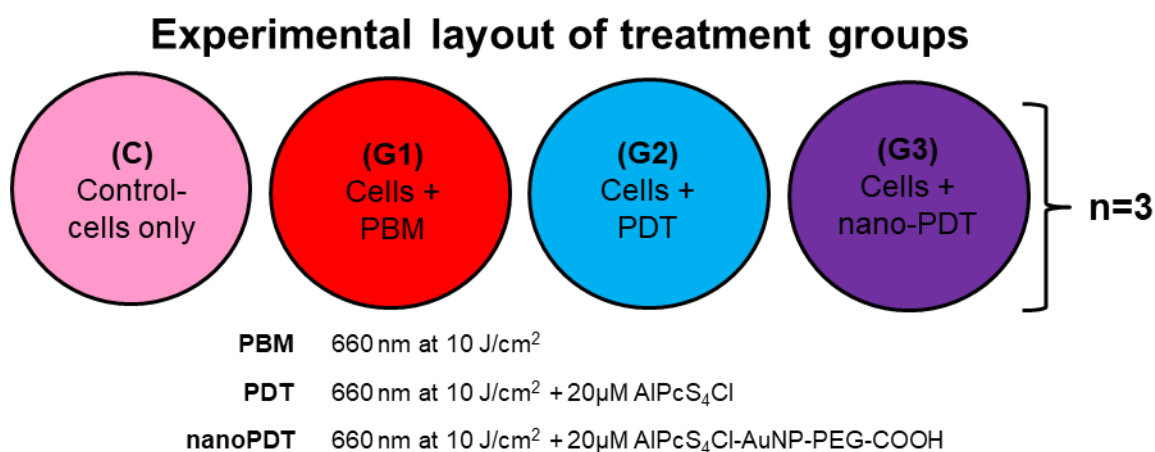
Figure 1. Layout of A549 lung cancer cells and PDT treatment experimental groups.

The cells were irradiated once 24 h after receiving the PS and PS-gold nano conjugate with a 660 nm Light Emitting Diode (LED, THOR Photomedicine, Buckinghamshire, UK) plate illuminator that facilitates the docking of a 6-well plate on top of the LED power source to irradiate cells from the bottom. The illuminator was fitted with a Keithley 2200-32-3 power supply (PSU, THOR Photomedicine, Buckinghamshire, UK). To eliminate nuisance factors, all trials were conducted in the dark at room temperature. Irradiation parameters are indicated in Table 1 below, where these parameters were standardised by the manufacturer.

Table 1. LED well plate illuminator parameters.

λ (nm)	V (volts)	A (amps)	Power (mW)	Intensity (mW/cm^2)	Fluence (J/cm^2)
6594	22,913	302	33,130	11,717	10

2.3. Morphology

Using inverted light microscopy (OLYMPUS CKX41, Tokyo, Japan) and an Olympus SC30 microscope-connected digital camera with the Olympus cellSens Software program, changes in morphology 24 h after irradiation were observed and analysed.

2.4. Migration

The central scratch method is a typical way of assessing cell motility in vitro [21]. The assay was performed using modified literature methods [22,23]. The migration of cells was determined using the 'central scratch' technique. Cells were cultured and maintained in petri dishes under physiological conditions. Prior to irradiation, a central scratch was formed using a sterile P-200 pipette tip. Migration was recorded 0, 24, and 48 h after irradiation using an inverted light microscope.

2.5. Proliferation and Cytotoxicity

Following treatment, ATP concentrations were measured to see how PDT and nanoPDT affected lung cancer cells' metabolism. An assay for cell proliferation (Promega, G7570, Madison, WI, USA) was used to assess intracellular ATP. The manufacturer's instructions were followed exactly. A Multilabel Counter (Perkin Elmer, VICTOR3TM, 1420, Waltham, MA, USA) read and measured luminous cellular ATP and displayed the results in relative light units (RLU).

Cell death and membrane damage allow LDH to be released from cells, which was used to calculate the toxicity. The manufacturer-recommended CytoTox96® nonradioactive cytotoxicity test (Promega, G400, Madison, WI, USA) was employed. Using a multilabel Counter at 490 nm, we assessed the formation of formazan indicative of cytotoxicity.

2.6. Cell Cycle Analysis—PI DNA Staining

Cell cycle analysis was performed using flow cytometry by quantitation of DNA content. Cells were fixed using 70% ethanol and washed. Cells were then treated using 50 μL RNase (stock 100 μg/mL) and stained with 200 μL Propidium iodide (PI) (stock solution 50 μg/mL). The stoichiometric dye PI binds in proportion to the amount of DNA present in the cell. For analysis using a flow cytometer (BD Accuri Flow Cytometer C6, BD Life Sciences, San Jose, CA, USA), a maximum of 10^3 events were recorded for each experimental sample; where the relevant cell population was gated, the gated samples were then applied in a histogram plot using the FL 2 channel with a 535/617 ex/em, where a right shift depicts an increase in fluorescence detection and a left shift a decrease, enabling the cells in the various phases to be depicted as percentage values. Thus, cells in the S phase have more DNA than cells in the G1 phase. They absorb proportionately more dye and fluoresce more brightly until their DNA content is doubled. G2 cells are roughly twice as luminous as G1 cells.

2.7. Cell invasion—Transwell

The QCM ECMatrix Cell Invasion Assay (Merck, ECM555, Darmstadt, Germany) was used to determine the invasion ability of the lung cancer cells using a technique based on the Boyden Chamber assay. Cells were cultured in serum-free media 24 h prior to the assay, as indicated by the manufacturer, harvested into ECM wells in serum-free media using 5×10^4 cells per well, and complete media was added to a feeder beneath the culture wells. Cells were then treated with PDT, whereafter, 24 h after the irradiation cells passed through, the matrix membrane was detached and identified using CyQuant GRdye (Merck, Darmstadt, Germany), where invasive cells were detected via fluorescence spectroscopy using a 480/520 nm filter set. A standard curve was generated to calculate the number of cells (x) that have passed through the ECM using the following equation: y = 143.8x − 0.364; where y was the fluorescence measured in RLUs.

2.8. Statistical Analysis

The migratory morphology data were statistically analysed using ImageJ, a free Java-based image processing system (National Institute of Health, Bethesda, MD, USA). All quantitative experiments were repeated three times (n = 3). Biochemical assays were done in duplicate, and the mean result was used for statistical analysis. All controls were included to ensure validity of the results. The Student T-test (difference between control and experimental group) was used for each independent variable, and ANOVA was measured to determine the differences between the various experimental groups. Results are represented in figures, tables, and/or graphs. Analysis indicating the statistical significance $p < 0.05$ (*), $p < 0.01$ (**), and $p < 0.001$ (***) and standard errors was done using Sigma plot 12.0 software.

3. Results

3.1. Morphology

During the in vitro PDT treatment of lung cancer cells, the cells undergo some structural morphological changes as an effect of the PBM and PDT treatments that are applied. The morphological effects observed using PBM on noncancerous cells had shown no structural changes, however an increase in cell density had been seen [23,24]. Similar morphological outcomes were seen when treating cancerous cells with PBM using a low fluence [25]. During cell death, the following morphological alterations can be observed, wherein the cytoplasm swells, organelles are destroyed, and the plasma membrane disintegrates, resulting in the outflow of intracellular contents during necrosis. On the contrary, apoptosis results in cell shrinkage, increased cytoplasmic and organelle packing, widespread plasma membrane blebbing, and the production of distinct apoptotic bodies that are phagocytized in vivo by macrophages or nearby normal cells [26]. Autophagy is the process through which the cytoplasm and organelles are enveloped in vacuoles called autophagosomes. The contents of autophagosomes are digested and recycled following fusion with lysosomes. Autophagy occurs sequentially and has distinct properties, and is thus considered a second type of planned cell death [27]. Cell death distinctions can be made by morphological changes by means of light microscopy [28]. Although the exact cell death mechanism for PDT and nanoPDT was not established, the morphological changes seen in Figure 2 were typical of lung cancer cells with no cell death induced for (a) the control kept in normal culture conditions and (b) PBM-treated cells, having a similar morphology to the control. Cells treated with (c) PDT and (d) nanoPDT showed indications of free-floating cells, cell shrinkage, and rounding up, morphologically simulating that of cell death. Programmed cell death, such as apoptosis, autophagy, and necrosis, plays crucial roles in metastatic processes, as cancer cells cannot metastasise without overcoming these various forms of cell death [29].
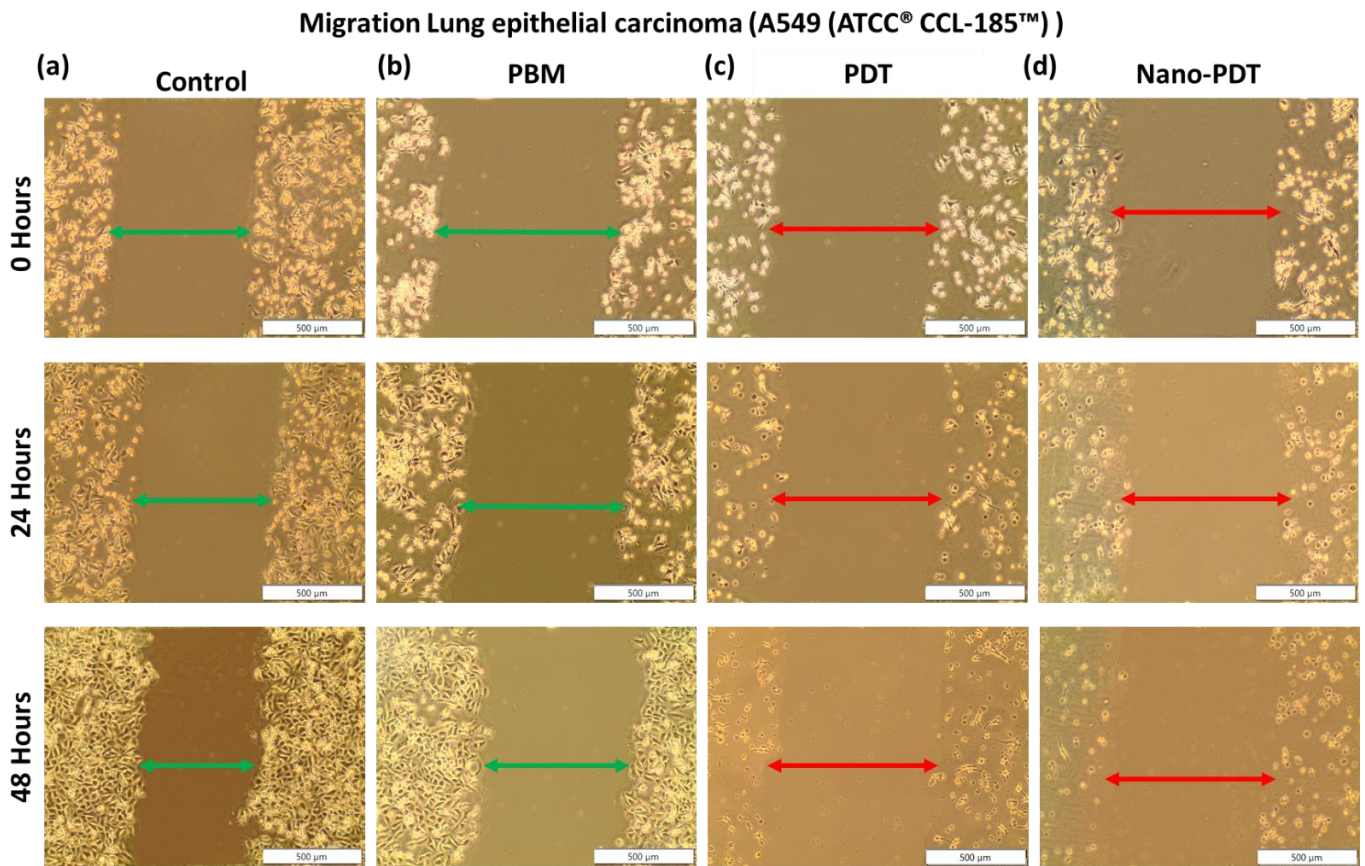
3.2. Migration

The scratch assay is an in vitro technique that has been extensively used in science to determine the contribution of molecular and cellular mechanisms to cell migration over the years [30]. The scratch test is conducted by creating a "scratch" in a monolayer of cells and photographing the cells at the start and at regular intervals throughout cell migration as the scratch closes. Figure 3 shows the migration of lung epithelial carcinoma cells (A549) at 0, 24, and 48 h post-PDT treatment. Untreated (a) control cells show slight motility towards the central scratch and (b) cells receiving PBM show signs of rapid migration where the cells move towards the central scratch and the cell density increases. Comparatively, cells treated with (c) PDT and (d) nanoPDT show a decreased migration rate and were not able to close the scratch over time, where dead cells and cell debris were seen floating in the culture medium due to cell arrest.
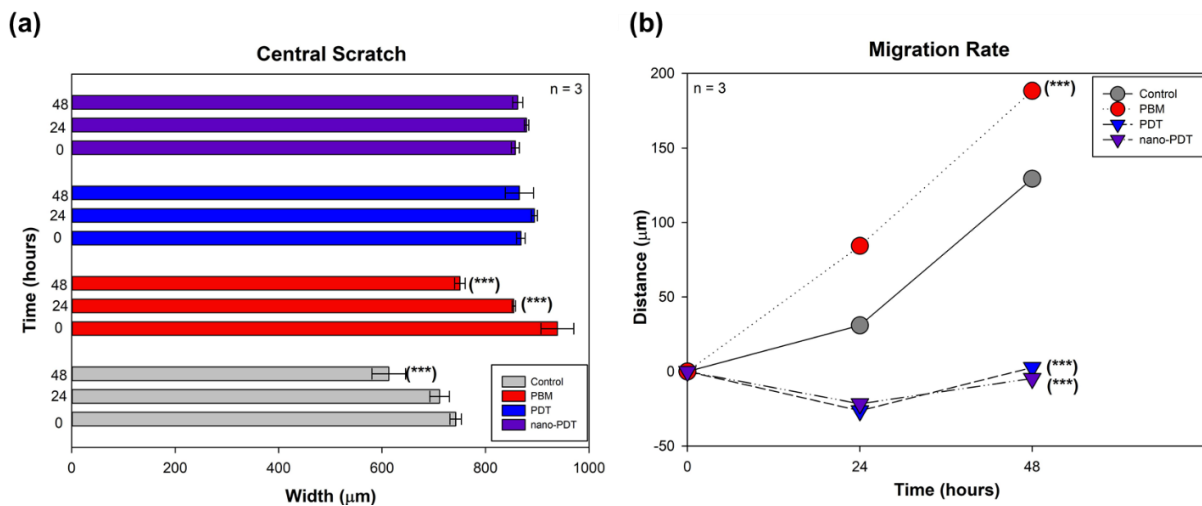
Lung epithelial carcinoma (A549 (ATCC® CCL-185™))
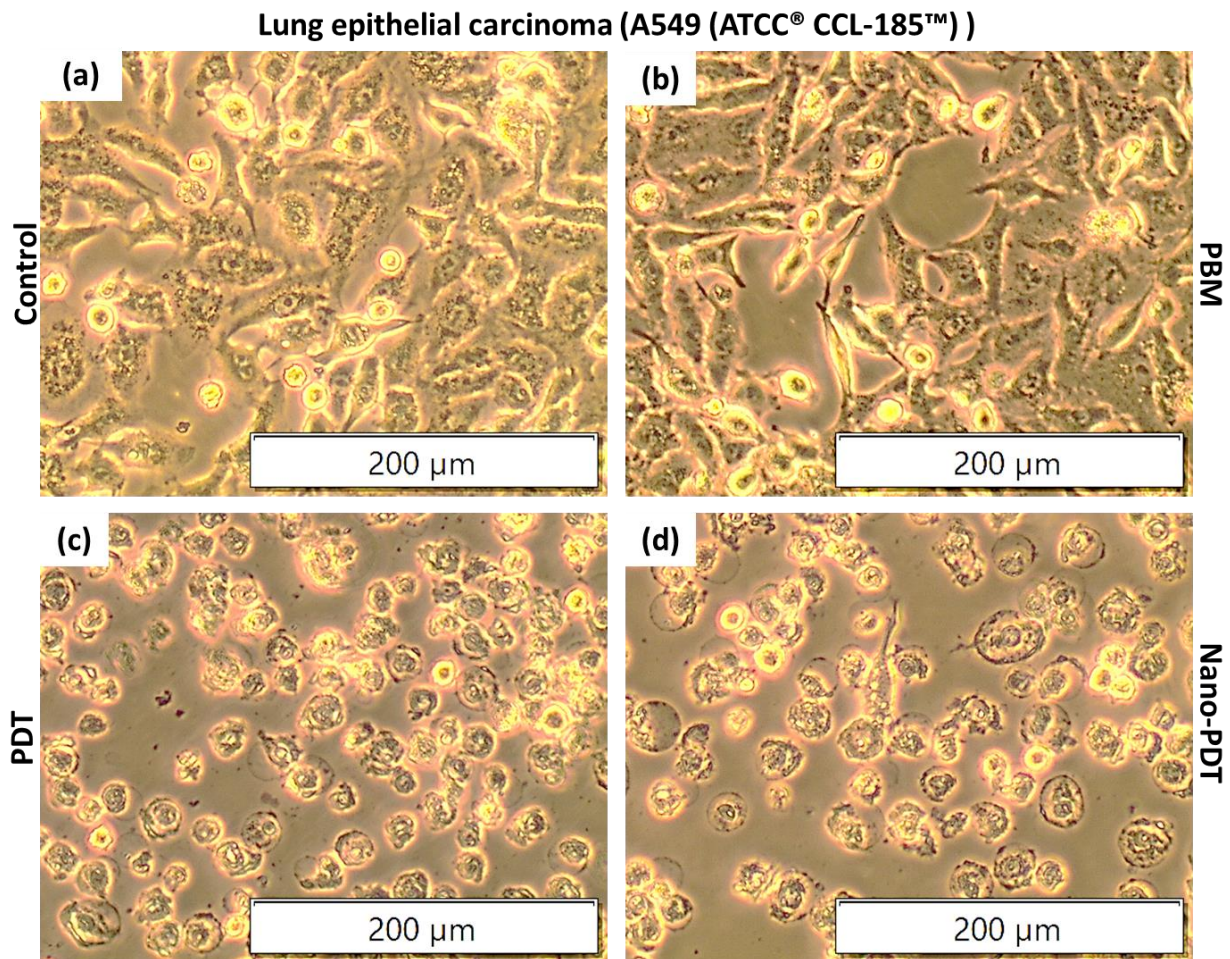
Figure 2. Morphology of lung epithelial carcinoma cells (A549) 24 h post-PDT treatment: (**a**) Control cells receiving no treatment. (**b**) Cells receiving PBM of 10 J/cm^2 with a wavelength of 660 nm. (**c**) Cells receiving PDT treatment using 20 μM AlPcS$_4$Cl and 10 J/cm^2 irradiation. (**d**) Cells receiving nanoPDT treatment using the AlPcS$_4$Cl-goldnano bioconjugate.

The analysis of migration morphology shows (Figure 4a) the measured scratch width over a period of 48 h, whereas the control shows a significant closure after 48 h, and PBM treatment groups indicate significant closure 24 and 48 h post-treatment of the central scratch over time, indicating enhanced migration because of PBM [21]. Cells treated with PDT and nanoPDT indicate no closure of the central scratch over time due to cell death. Similarly, the migration rate of the cells (Figure 4b) measured over time indicate that there was a significant increase in migration for cells treated with PBM alone, indicating the proliferative and motility effects of PBM induced on cells [21], whereas PDT- and nanoPDT-treated cells both showed significant decreases in the distance the cells can travel. It is seen that lung cancer cells treated with PDT and nanoPDT were unable to close the central scratch, negating the proliferative effects and decreasing cellular migration due to cell death induction caused by PDT.

Figure 3. Migration morphology of lung epithelial carcinoma cells (A549) at 0, 24, and 48 h post-PDT treatment: (**a**) Control cells receiving no treatment. (**b**) Cells receiving PBM of 10 J/cm^2 with a wavelength of 660 nm. (**c**) Cells receiving PDT treatment using 20 μM AlPcS$_4$Cl and 10 J/cm^2 irradiation. (**d**) Cells receiving nanoPDT treatment using the AlPcS$_4$Cl-goldnano bioconjugate.
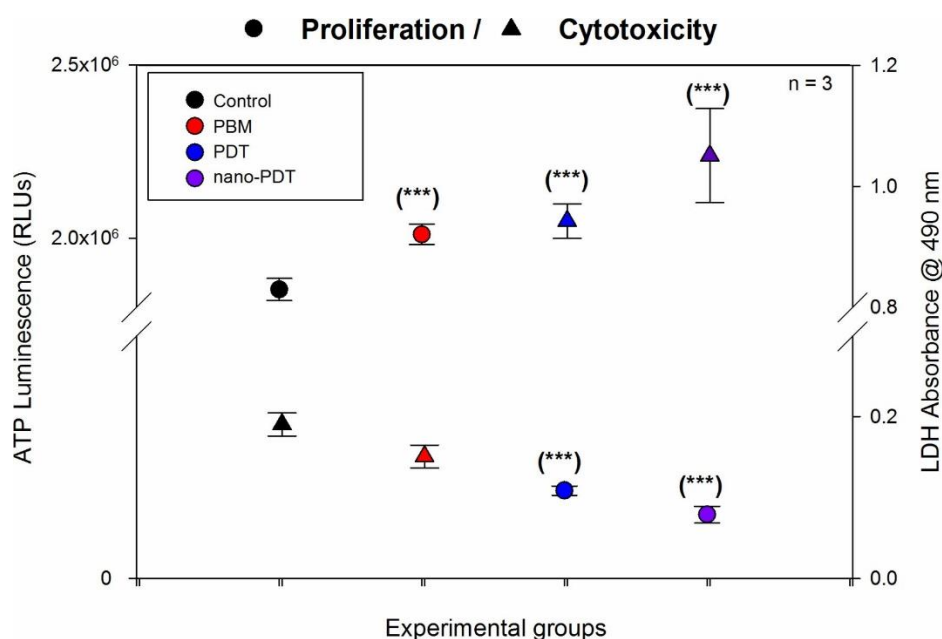

Figure 4. Migration analysis of lung epithelial carcinoma cells (A549) at 0, 24, and 48 h post-PDT treatment: (**a**) Central scratch width of experimental samples over time. (**b**) Migration rate indicating the distance (μm) the cells travelled over time.

3.3. Proliferation and Cytotoxicity

Cell proliferation was measured using ATP luminescence in relative light units and cytotoxicity was measured as the amount of LDH leakage caused by membrane damage and

cell death, where it was read using an absorbance of 490 nm. Proliferation results (Figure 5) show that control cells and PBM-treated cells had an increased proliferation rate, with PBM cells having a significant increase in proliferation. Cells treated with PDT and nanoPDT had a significant decrease in proliferation compared to the control and cells treated with PBM alone. There was a slight decrease seen in cells treated with nanoPDT compared to PDT, however this decrease was not significant. Cytotoxicity results show that control cells and PBM-treated samples released little LDH into the environment, and that cells treated with PDT and nanoPDT both released significant amounts of LDH. Additionally, nanoPDT-treated samples showed a higher increase in LDH release when compared to PDT-treated samples.

Figure 5. Proliferation and cytotoxicity of lung epithelial carcinoma cells (A549) 24 h post-PDT treatment.

3.4. Cell Cycle Analysis—PI DNA Staining

The cell cycle phases were identified by quantifying cellular DNA. The cell cycle is a multifaceted process during which cells proliferate. It consists of the gap 1, or G1, the stage where cells mature. The S phase, where the cell copies its DNA; the G2 phase, where cells prepare to divide and perform DNA checks; and the M phase, where cells undergo mitoses. Cells can also move into the G0 phase, indicative of cell cycle arrest or cell death. Results in Figure 6 show that the (a) control cells and (b) PBM-treated cells are predominantly in the G1 and S phase. Whereas (c) PDT-treated samples show many cells entering G0, where the percentage of cells in G1 decreased, as well as the cells moving out of S phase. Cells treated using (d) nanoPDT shows an even greater cell cycle arrest, with no cells seen in S phase and less cells in G1 compared to PDT.

3.5. Cell invasion—Transwell

The ability of lung cancer to spread metastatically was determined by ECM invasion, where a rise in fluorescence indicates invasion and a decrease indicates reduced invasiveness. Figure 7 shows the cellular fluorescence and Table 2 shows the percentage of cells relative to the initial cell seeding amount that have passed through the ECM. The control sample shows the spontaneous migration of lung cancer cells indicating the metastatic nature of lung cancer with a mean fluorescent measurement of 714,685 RLUs, where 9.9% of the cells initially seeded passed through the ECM. When comparing the treated samples to the control, it is seen that cells treated with PBM (17917 RLUs) have a significant decrease

in their invasion abilities, more so than the PDT-treated samples, where only 0.2% of cells passed through the ECM. This phenomenon is ascribed to the increase in proliferation that is seen during lung cancer cell PBM treatment, where the cells tend to rather proliferate than invade during the process [31]. Lung cancer cells treated with PDT (588916 RLUs) and nanoPDT (498938 RLUs) show a significantly decreased ability to invade the ECM post-treatment compared to the untreated control, indicated by a decrease in the fluorescence of the RLUs measured, where 8% and 6.9% of PDT- and nanoPDT-treated cells passed through the ECM, respectively. The decrease in cell invasion was more significant for nanoPDT-treated samples. This indicates that PDT and nanoPDT more so has a debilitating effect on the invasive and metastatic properties of lung cancer cells.
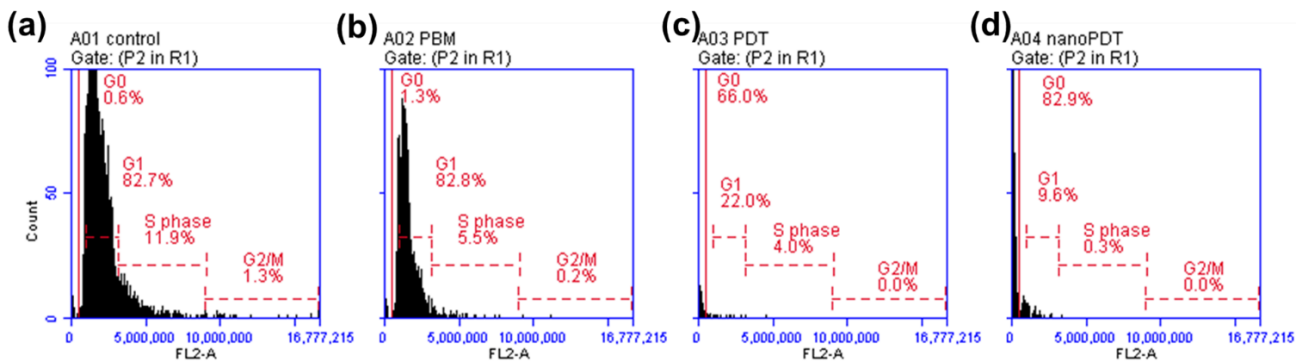
Figure 6. Cell cycle analysis through DNA quantification using flow cytometry of lung epithelial carcinoma cells (A549) 24 h post-PDT treatment: (**a**) Control cells receiving no treatment. (**b**) Cells receiving PBM of 10 J/cm^2 with a wavelength of 660 nm. (**c**) Cells receiving PDT treatment using 20 μM AlPcS4Cl and 10 J/cm^2 irradiation. (**d**) Cells receiving nanoPDT treatment using the AlPcS$_4$Cl-goldnano bioconjugate.
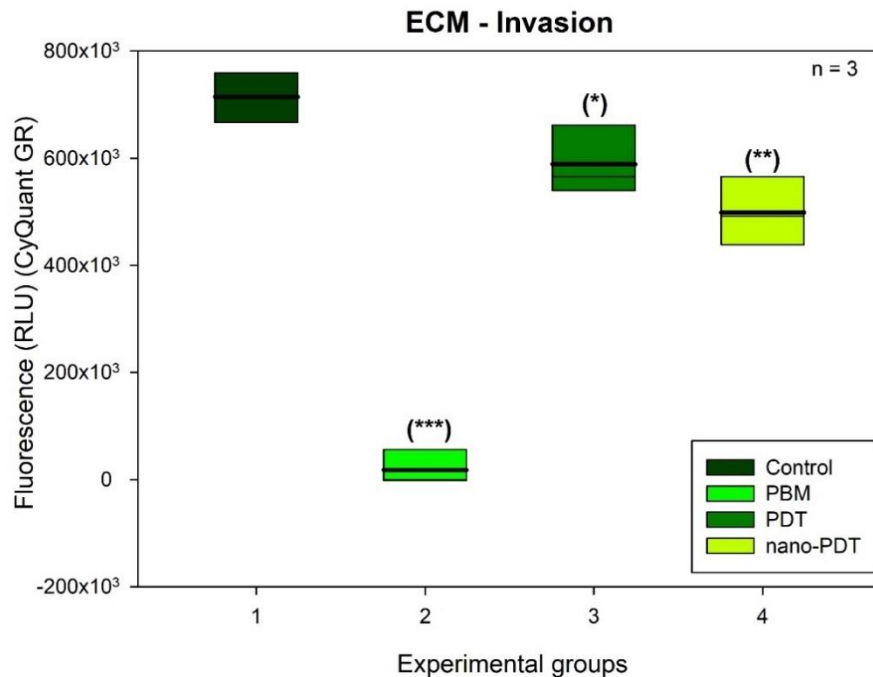
Figure 7. ECM cell invasion assay of lung epithelial carcinoma cells (A549) 24 h post-PDT treatment.

Table 2. ECM data of A549 lung cancer cells 24 h post-PDT treatment. The standard (Std) was obtained using the initial cell seeding concentration of 5×10^4 that represents 100% cell invasion. The concentration of cells that passed through the ECM were calculated, as was the percentage of cells that passed through the ECM compared to the Std.

	Fluorescence in RLUs	Cell Concentration	Percentage (%)
Std	7,190,218	50,000.00	100
Control	714,685	4969.84	9.94
PBM	17,917	124.59	0.25
PDT	588,916	4095.25	8.19
nanoPDT	498,938	3469.56	6.94

4. Discussion

Initially, it was believed that PDT killed cells by necrosis. Several investigations have demonstrated that apoptosis may be induced in a range of cell types using a variety of different sensitizers and pathways. PDT treatment that induces cell death primarily by apoptosis is very desirable for medical applications, since it is less hazardous to patients and does not trigger further inflammatory responses [28]. Morphology showed that PDT and nanoPDT bodes well for lung cancer cell antimetastatic effects seen by the observations of cells death. However, the favoured cell death mode, considering future clinical application, needs to be established where the mechanism of cell death can be confirmed by experiments that highlight the activation of cell death processes; for example, the apoptotic process can be identified using Acridine Orange staining and the expression of apoptotic markers such as matrix metalloproteinase 3 activation and annexin VPI staining. It can be confirmed that the morphological cell death observed was due to PDT alone, as previous studies have indicated that the use of AuNPs alone and with photoactivation had no morphological effects on the cells [19,32], however the use of AuNPs as a delivery vehicle of PSs had no detrimental effects to the treatments and might have enhanced the PDT effects, as seen in the continuing studies. Therefore, AuNPs can be used as a delivery vehicle for PDT by passively enhancing the PS uptake. Migration is a malignant hallmark for cancer metastasis [33]. Considering lung cancer's ability to metastasize, cancer treatments need to be effective in reducing cell motility and their proliferative abilities, which can reduce cancer relapse and enhance prognosis. The interruption of normal biological function followed by disseminating tumour cells causes mortality and morbidity in individuals with cancers. Cancer metastasis is thought to be caused by tumour cell motility. The importance of tumour cell migration in metastatic development has been demonstrated experimentally and empirically through fundamental and clinical studies. Cell motility is seldom targeted clinically, and adjuvant treatment to prevent cancer cell spread is severely restricted [34]. The purpose of this study was to determine the effect of nanoPDT on lung cancer cell metastatic abilities. It is seen that PDT and nanoPDT greatly decreased the ability of lung cancer cells to metastasise, indicated by a decrease in cell migration.

Cancer cells must be both proliferative and invasive to infiltrate and metastasize. Proliferation is involved in secondary tumour formation once cancer has invaded or migrated to a new location [1]. Avoiding secondary tumour formation may improve the prognosis for certain types of cancer, particularly lung cancer, which has been documented to produce secondary tumour formation [35]. It has been discovered that treatment can cure secondary cancer only in a tiny percentage of cases, where it has been established that secondary malignancies are incurable, and that the strategy of treatment should be focused on controlling the disease or managing any symptoms. We observed significant reductions in lung cancer cell proliferation following PDT and nanoPDT treatment in our investigation. The decrease in proliferation is also directly linked to the cells' viability, as the assay measures ATP generation, and nonviable cells cease production of ATP [36], which, with a diminished cell metabolism, result in the cells' decreased metastatic potential. Additionally, demonstrating

nanoPDT's efficacy is the nanoparticle-enhanced toxicity. Research has shown that using NPs can increase treatment selectivity, lower effective treatment dose, enhance passive drug uptake, promote solubility and stability, and reduce dark toxicity [37]. In this instance, the use of AuNPs as a delivery vehicle for the delivery of AlPcS$_4$Cl is suggested to enhance the PS solubility and therefore their passive uptake into the cells due to their hydrophilic nature [38]. Lung cancer's proliferative, invasive, and migratory properties are correlated to the cell cycle phase they are in [39]. Cancer cell cycle arrest in the G1 phase is required for cell invasion [40] and cells in the S phase are indicative of proliferative activity [39,41]. Cells that are in the G0 phase or are senescent are unable to begin the cycle due to DNA damage and self-destruction [42,43]. Invasion via the extracellular matrix (ECM) is an essential phase in tumour metastasis [44]. Cancer cells initiate invasion by adhering to and extending along the blood vessel wall. Proteolytic enzymes, such as matrix metalloproteinases (MMP) collagenases, create tiny holes in the sheath-like membrane, covering the blood vessels to allow cancer cells to enter the bloodstream [45]. Previous studies have demonstrated that proliferation and invasion are two contrasting events in some certain conditions, and tumour cells can switch between these two states [31,46]. This was observed when the lung cancer cell cycle and ECM invasion were examined. The results indicated that untreated control lung cancer cells remained predominantly in the G0/S phase and invaded the ECM, whereas, when stimulated with PBM, lung cancer cells appeared to be less invasive, with a significant decrease in ECM invasion and a significant increase in proliferation. However, when lung cancer cells were treated with PDT, they demonstrated a significant decrease in ECM invasion, decreased proliferation, and increased membrane damage caused by cytotoxicity, indicating that the cells entered the G0 phase. Additionally, a bigger significance in terms of decreased ECM invasion was observed along with lung cancer cell cycle arrest, in which cells exit the G1/S stages of invasion and proliferation and enter irreversible G0 owing to the severe cytotoxicity and cellular degradation caused when nanoPDT was used.

5. Conclusions

The regulatory criteria for cancer treatment include the need for the drug to be cytostatic, producing antiproliferation and toxicity in the cancer, as research indicates that therapy-induced senescence offers a unique functional target that may enhance cancer therapy [47]. The preliminary findings in this study show that phototherapy, using an AlPcS$_4$Cl-goldnano bioconjugate, prevents lung cancer migration and invasion, induces cell cycle arrest, and reduces the proliferative abilities of human lung cancer cells (A549; (ATCC® CCL-185™, Manassas, VA, USA)). Hence, the result suggests that phototherapy with gold nanoparticles could be a promising agent to reduce the invasiveness and metastatic abilities of lung cancer cells and is an effective cytostatic treatment for lung cancer cells, as demonstrated by a significant reduction in proliferation and an increase in toxicity. However, due to the preliminary nature of the study, further experiments on the exact mechanisms underlying the inhibition of lung cancer cells' migration induced by nanoPDT need to be carried out. To further overcome any methodological limitations from this study, experiments including the evaluation of cellular migration after 48 h can be explored to determine whether the nanoPDT effects are irreversible, along with evaluating whether ECM stiffness can influence the mechanisms of cell metastasis due to healthy and diseased tissue having various degrees of stiffness.

References

1. Martin, T.A.; Ye, L.; Sanders, A.J.; Lane, J.; Jiang, W.G. Cancer invasion and metastasis: Molecular and cellular perspective. In *Madame Curie Bioscience Database*; Landes Bioscience: Austin, TX, USA, 2013.
2. Sung, H.; Ferlay, J.; Siegel, R.L.; Laversanne, M.; Soerjomataram, I.; Jemal, A.; Bray, F. Global cancer statistics 2020: GLOBOCAN estimates of incidence and mortality worldwide for 36 cancers in 185 countries. *CA Cancer J. Clin.* **2021**, *71*, 209–249. [CrossRef]
3. Martins, D.; Mendes, F.; Schmitt, F. Microbiome: A supportive or a leading actor in lung cancer? *Pathobiology* **2021**, *88*, 193–202. [CrossRef]
4. Marques, E.C.P.; Lopes, F.P.; Nascimento, I.C.; Morelli, J.; Pereira, M.V.; Meiken, V.M.M.; Pinheiro, S.L. Photobiomodulation and photodynamic therapy for the treatment of oral mucositis in patients with cancer. *Photodiagn. Photodyn. Ther.* **2020**, *29*, 101621. [CrossRef] [PubMed]
5. De Freitas, L.F.; Hamblin, M.R. Proposed mechanisms of photobiomodulation or low-level light therapy. *IEEE J. Sel. Top Quantum Electron.* **2016**, *22*, 348–364. [CrossRef] [PubMed]
6. Gunaydin, G.; Gedik, M.E.; Ayan, S. Photodynamic therapy—Current limitations and novel approaches. *Front. Chem.* **2021**, *9*, 400. [CrossRef] [PubMed]
7. Dos Santos, A.F.; de Almeida, D.R.Q.; Ferreira Terra, L.; Baptista, M.S.; Labriola, L. Photodynamic therapy in cancer treatment—An update review. *J. Cancer Metastas. Treat.* **2019**, *5*, 25. [CrossRef]
8. Amin, R.M.; Hauser, C.; Kinzler, I.; Rueck, A.; Scalfi-Happ, C. Evaluation of photodynamic treatment using aluminum phthalocyanine tetrasulfonate chloride as a photosensitizer: New approach. *Photochem. Photobiol. Sci.* **2012**, *11*, 1156–1163. [CrossRef] [PubMed]
9. Sekkat, N.; Van Den Bergh, H.; Nyokong, T.; Lange, N. Like a bolt from the blue: Phthalocyanines in biomedical optics. *Molecules* **2012**, *17*, 98–144. [CrossRef]
10. Kruger, C.A.; Abrahamse, H. Utilisation of targeted nanoparticle photosensitiser drug delivery systems for the enhancement of photodynamic therapy. *Molecules* **2018**, *23*, 2628. [CrossRef]
11. Patra, J.K.; Das, G.; Fraceto, L.F.; Campos, E.V.R.; del Pilar Rodriguez-Torres, M.; Acosta-Torres, L.S.; Diaz-Torres, L.A.; Grillo, R.; Swamy, M.K.; Sharma, S.; et al. Nano based drug delivery systems: Recent developments and future prospects. *J. Nanobiotechnol.* **2018**, *16*, 71. [CrossRef]
12. Cheng, Z.; Li, M.; Dey, R.; Chen, Y. Nanomaterials for cancer therapy: Current progress and perspectives. *J. Hematol. Oncol.* **2021**, *14*, 1–27. [CrossRef] [PubMed]
13. Rout, G.K.; Shin, H.-S.; Gouda, S.; Sahoo, S.; Das, G.; Fraceto, L.F.; Patra, J.K. Current advances in nanocarriers for biomedical research and their applications. *Artif. Cells Nanomed. Biotechnol.* **2018**, *46*, 1053–1062. [CrossRef]
14. Khan, I.; Saeed, K.; Khan, I. Nanoparticles: Properties, applications and toxicities. *Arab. J. Chem.* **2019**, *12*, 908–931. [CrossRef]
15. Solati, E.; Dorranian, D. Comparison Between silver and gold nanoparticles prepared by pulsed laser ablation in distilled water. *J. Clust. Sci.* **2014**, *26*, 727–742. [CrossRef]
16. Phan, H.T. Haes, A.J. What does nanoparticle stability mean? *J. Phys. Chem. C* **2019**, *123*, 16495–16507. [CrossRef]
17. Arvizo, R.; Bhattacharya, R.; Mukherjee, P. Gold nanoparticles: Opportunities and challenges in nanomedicine. *Expert Opin. Drug Deliv.* **2010**, *7*, 753–763. [CrossRef] [PubMed]

18. Vines, J.B.; Yoon, J.-H.; Ryu, N.-E.; Lim, D.-J.; Park, H. Gold nanoparticles for photothermal cancer therapy. *Front. Chem.* **2019**, *7*, 167. [CrossRef] [PubMed]

19. Crous, A.; Abrahamse, H. Effective gold nanoparticle-antibody-mediated drug delivery for photodynamic therapy of lung cancer stem cells. *Int. J. Mol. Sci.* **2020**, *21*, 3742. [CrossRef]

20. Crous, A.; Kumar, S.S.D.; Abrahamse, H. Effect of dose responses of hydrophilic aluminium (III) phthalocyanine chloride tetrasulphonate based photosensitizer on lung cancer cells. *J. Photochem. Photobiol. B Biol.* **2019**, *194*, 96–106. [CrossRef]

21. Jere, S.W.; Houreld, N.N.; Abrahamse, H. Effect of photobiomodulation on cellular migration and survival in diabetic and hypoxic diabetic wounded fibroblast cells. *Lasers Med. Sci.* **2020**, *36*, 365–374. [CrossRef]

22. Ayuk, S.M.; Abrahamse, H.; Houreld, N.N. The role of photobiomodulation on gene expression of cell adhesion molecules in diabetic wounded fibroblasts in vitro. *J. Photochem. Photobiol. B Biol.* **2016**, *161*, 368–374. [CrossRef] [PubMed]

23. Crous, A.; van Rensburg, M.J.; Abrahamse, H. Single and consecutive application of near-infrared and green irradiation modulates adipose derived stem cell proliferation and affect differentiation factors. *Biochimie* **2021**. [CrossRef] [PubMed]

24. Mokoena, D.R.; Houreld, N.N.; Kumar, S.S.D.; Abrahamse, H. Photobiomodulation at 660 nm stimulates fibroblast differentiation. *Lasers Surg. Med.* **2020**, *52*, 671–681. [CrossRef] [PubMed]

25. Crous, A.; Abrahamse, H. Aluminium (III) phthalocyanine chloride tetrasulphonate is an effective photosensitizer for the eradication of lung cancer stem cells. *R. Soc. Open Sci.* **2021**, *8*, 210148. [CrossRef]

26. Kar, B.; Sivamani, S. Apoptosis: Basic concepts, mechanisms and clinical implications. *Int. J. Pharm. Sci. Res.* **2015**, *6*, 940.

27. Parzych, K.R.; Klionsky, D.J. An overview of autophagy: Morphology, mechanism, and regulation. *Antioxidants Redox Signal.* **2014**, *20*, 460–473. [CrossRef]

28. Belashov, A.V.; Zhikhoreva, A.A.; Belyaeva, T.N.; Nikolsky, N.N.; Semenova, I.V.; Kornilova, E.S.; Vasyutinskii, O.S. Quantitative assessment of changes in cellular morphology at photodynamic treatment in vitro by means of digital holographic microscopy. *Biomed. Opt. Express* **2019**, *10*, 4975–4986. [CrossRef]

29. Su, Z.; Yang, Z.; Xu, Y.; Chen, Y.; Yu, Q. Apoptosis, autophagy, necroptosis, and cancer metastasis. *Mol. Cancer* **2015**, *14*, 48. [CrossRef]

30. Bobadilla, A.V.P.; Arévalo, J.; Sarró, E.; Byrne, H.M.; Maini, P.K.; Carraro, T.; Balocco, S.; Meseguer, A.; Alarcón, T. In vitro cell migration quantification method for scratch assays. *J. R. Soc. Interface* **2019**, *16*, 20180709. [CrossRef]

31. Yan, M.; Yang, X.; Shen, R.; Wu, C.; Wang, H.; Ye, Q.; Yang, P.; Zhang, L.; Chen, M.; Wan, B.; et al. miR-146b promotes cell proliferation and increases chemosensitivity, but attenuates cell migration and invasion via FBXL10 in ovarian cancer. *Cell Death Dis.* **2018**, *9*, 1123. [CrossRef]

32. Soenen, S.J.; Manshian, B.; Montenegro, J.M.; Amin, F.; Meermann, B.; Thiron, T.; Cornelissen, M.; Vanhaecke, F.; Doak, S.; Parak, W.J.; et al. Cytotoxic effects of gold nanoparticles: A multiparametric study. *ACS Nano* **2012**, *6*, 5767–5783. [CrossRef]

33. Tahtamouni, L.; Ahram, M.; Koblinski, J.; Rolfo, C. Molecular regulation of cancer cell migration, invasion, and metastasis. *Anal. Cell. Pathol.* **2019**, *2019*, 1356508. [CrossRef]

34. Anderson, R.L.; Balasas, T.; Callaghan, J.; Coombes, R.C.; Evans, J.; Hall, J.A.; Kinrade, S.; Jones, D.; Jones, P.S.; Jones, R.; et al. A framework for the development of effective anti-metastatic agents. *Nat. Rev. Clin. Oncol.* **2019**, *16*, 185–204. [CrossRef]

35. Zhu, T.; Bao, X.; Chen, M.; Lin, R.; Zhuyan, J.; Zhen, T.; Xing, K.; Zhou, W.; Zhu, S. Mechanisms and future of non-small cell lung cancer metastasis. *Front. Oncol.* **2020**, *10*, 2441. [CrossRef]

36. Kim, S.-Y. Cancer energy metabolism: Shutting power off cancer factory. *Biomol. Ther.* **2018**, *26*, 39. [CrossRef]

37. Hodgkinson, N.; Kruger, A.C.; Abrahamse, H. Targeted photodynamic therapy as potential treatment modality for the eradication of colon cancer and colon cancer stem cells. *Tumor Biol.* **2017**, *39*, 1010428317734691. [CrossRef] [PubMed]

38. Huang, B.; Cohen, J.R.; I Fernando, R.; Hamilton, D.H.; Litzinger, M.T.; Hodge, J.W.; Palena, C. The embryonic transcription factor Brachyury blocks cell cycle progression and mediates tumor resistance to conventional antitumor therapies. *Cell Death Dis.* **2013**, *4*, e682. [CrossRef] [PubMed]

39. Eymin, B.; Gazzeri, S. Role of cell cycle regulators in lung carcinogenesis. *Cell Adhes. Migr.* **2010**, *4*, 114–123. [CrossRef] [PubMed]

40. Bayarmagnai, B.; Perrin, L.; Pourfarhangi, K.E.; Graña, X.; Tüzel, E.; Gligorijevic, B. Invadopodia-mediated ECM degradation is enhanced in the G1 phase of the cell cycle. *J. Cell Sci.* **2019**, *132*, jcs227116. [CrossRef] [PubMed]

41. Barr, A.R.; Cooper, S.; Heldt, F.S.; Butera, F.; Stoy, H.; Mansfeld, J.; Novak, B.; Bakal, C. DNA damage during S-phase mediates the proliferation-quiescence decision in the subsequent G1 via p21 expression. *Nat. Commun.* **2017**, *8*, 14728. [CrossRef]

42. Niederhuber, J.E.; Armitage, J.O.; Doroshow, J.H.; Kastan, M.B.; Tepper, J.E. Control. of the cell cycle. In *Abeloff's Clinical Oncology*; Churchill Livingstone: Philadelphia, PA, USA, 2014; pp. 52–68.

43. Kumari, R.; Jat, P. Mechanisms of cellular senescence: Cell cycle arrest and senescence associated secretory phenotype. *Front. Cell Dev. Biol.* **2021**, *9*, 485. [CrossRef] [PubMed]

44. Kai, F.; Drain, A.P.; Weaver, V.M. The extracellular matrix modulates the metastatic journey. *Dev. Cell* **2019**, *49*, 332–346. [CrossRef] [PubMed]

45. Quintero-Fabián, S.; Arreola, R.; Becerril-Villanueva, E.; Torres-Romero, J.C.; Arana-Argáez, V.; Lara-Riegos, J.; Ramírez-Camacho, M.A.; Alvarez-Sánchez, M.E. Role of matrix metalloproteinases in angiogenesis and cancer. *Front. Oncol.* **2019**, *9*, 1370. [CrossRef] [PubMed]

46. Hur, H.; Lee, J.-Y.; Yang, S.; Kim, J.M.; Park, A.E.; Kim, M.H. HOXC9 induces phenotypic switching between proliferation and invasion in breast cancer cells. *J. Cancer* **2016**, *7*, 768–773. [CrossRef] [PubMed]

47. Prasanna, P.G.; Citrin, E.D.; Hildesheim, J.; Ahmed, M.M.; Venkatachalam, S.; Riscuta, G.; Xi, D.; Zheng, G.; van Deursen, J.; Goronzy, J.; et al. Therapy-induced senescence: Opportunities to improve anticancer therapy. *J. Natl. Cancer Inst.* **2021**, *113*, 1285–1298. [CrossRef]